Progress In Electromagnetics Research, Vol. 143, 405–419, 2013

EARLY STAGE BREAST CANCER DETECTION USING INDIRECT MICROWAVE HOLOGRAPHY

Michael Elsdon*, Okan Yurduseven, and David Smith

Faculty of Engineering and Environment, Northumbria University, Newcastle upon Tyne, NE1 8ST, United Kingdom

Abstract—A novel microwave imaging approach for early stage breast cancer detection is described. The proposed technique involves the use of an Indirect Microwave Holographic technique employing a patented synthetic reference wave. This approach offers benefits in terms of simplicity, expense, comfort and safety when compared to current mammography techniques. Experimental results using a simulated breast phantom are included to demonstrate the validity of this technique to obtain 2D images. The technique is then extended to demonstrate the possibility of obtaining 3D images by using indirect stereoscopic holographic imaging.

1. INTRODUCTION

Breast cancer affects many women, and early detection and timely medical intervention is the key to long term survival and life quality for patients. X-ray mammography is currently the most effective technique for breast screening. However, approximately 10–30% of breast cancers are missed by mammography. Concerns have also been reported about the high number of false positives in screening mammograms [1]. A further disadvantage of this screening technique is the difficulty in imaging women with dense breasts [2]. Moreover, the ionising properties of X-rays place a restriction on the frequency of screening. These limitations motivate the search for new methods of breast tumor detection.

Microwave imaging of breast tumors offers an alternate method of breast cancer detection and has been the subject of much study [3–13]. Whilst X-ray mammography operates by detecting structural changes in the breast, microwave imaging operates by exploiting the

Received 17 September 2013, Accepted 6 November 2013, Scheduled 18 November 2013
* Corresponding author: Michael Elsdon (michael.elsdon@northumbria.ac.uk).

dielectric contrast between malignant and normal breast tissues at microwave frequencies. It is widely reported that dielectric changes in the breast occur before structural changes, which makes microwave imaging a potentially earlier detection method [10]. Under microwave radiation, the dielectric response of the malignant breast tissue demonstrates considerable differences in comparison to the normal breast tissue. This results in an increase in the level of backscattered signal from the malignancy within the breast tissue. Consequently, microwave imaging can potentially offer earlier detection of breast cancer. Microwave imaging is also more attractive to patients, as it is non-ionizing and breast compression is avoided, resulting in safer and more comfortable examinations. This technique also has the potential to be both sensitive and specific, to detect small tumors, and to be less expensive than methods such as MRI and nuclear medicine [8]. In view of this, microwave imaging of the human body for the purpose of cancer detection have been of interest for many years. Improvements in microwave hardware, imaging algorithms and computational speed have renewed interest in this area and made some applications feasible [14].

The use of microwave or millimetre waves for breast cancer detection is now an active area of research [3–13]. The majority of these approaches operate using direct techniques requiring the use of expensive vector measurement equipment to record the complex field scattered (microwave tomographic imaging) or reflected (confocal microwave imaging) from the breast tissue. The research detailed in this paper is based upon an Indirect Microwave Holographic Imaging approach. This method differs from the direct methods in that the complex field is not measured directly but recovered from scalar measurements performed using a low-cost power meter in a two stage process; the production of a holographic intensity pattern and the image reconstruction. This significantly simplifies the hardware implementation. In comparison to the use of a pulsed technique [9], the Indirect Microwave Holographic Imaging approach uses continuous wave (CW) signals which reduces its cost by a factor of up to six [15]. Central to this technique is the use of a Synthesised Reference Beam developed and patented at Northumbria University [16]. Initial results using a novel microwave imaging technique for the early detection of breast cancer has been reported [17], with experimental results obtained using a crude breast phantom. The focus of this paper is to extend this work and focus on recent experimental results using a modified breast phantom, which includes the effect of a skin layer. Moreover, Indirect Stereoscopic Holographic Imaging, which is capable of providing 3D images of scanned objects, is demonstrated for the first

time in the literature.

The remainder of this paper will be divided as follows: Section 2 presents a brief overview of the direct holographic approach. Section 3 describes the indirect holographic approach. Section 4 illustrates the application of microwave indirect holography to breast cancer detection. Section 5 outlines Indirect Stereoscopic Microwave Holography, highlighting the obtained results. A conclusion is presented in Section 6.

2. DIRECT HOLOGRAPHY

The use of Direct Holography for the determination of antenna radiation patterns and imaging of aperture fields has received much attention [18]. The same technique can also be adapted to reconstruct 3D images of objects from complex near field measurements. For the imaging of objects, a complex field pattern, $E(x, y)$, is recorded using expensive vector measurement equipment over a 2D aperture located at a distance, $z = d$, from the object. Performing a Fourier transform on this field converts the data to a plane wave spectrum (PWS), $A(k_x, k_y)$.

$$A(k_x, k_y) = F\{E(x, y)\} = \frac{1}{2\pi} \iint E(x, y) e^{-j(k_x \cdot x + k_y \cdot y)} dx \cdot dy \quad (1)$$

Assuming that the original coordinate system is located at the plane of the scanning aperture, $z = 0$, the complex scattered field at the plane, $E(x, y, z = d)$, can be obtained using a back-propagation approach [19].

$$E(x, y, z = d) = \frac{1}{2\pi} \iint A(k_x, k_y) \cdot e^{jk_z \cdot d} e^{-j(k_x \cdot x + k_y \cdot y)} dk_x \cdot dk_y \quad (2)$$

where,

$$k_z = \sqrt{k_0^2 \left(k_x^2 + k_y^2\right)} \quad (3)$$

3. INDIRECT MICROWAVE HOLOGRAPHY

The imaging technique adopted in this paper is based upon an Indirect Microwave Holographic Imaging approach, central to which is the use of a Synthesised Reference Beam. This approach was originally developed for determining the complex aperture fields of antennas without using vector measurement equipment [20] and subsequently extended for imaging of metallic objects [21]. For the detection of metal objects, it was shown that the image can be reconstructed from amplitude measurements taken with a low-cost power meter. For

application to breast cancer detection, there is only a small difference in the level of back scattered radiation. Previous work [22] has shown that measuring phase information of the field can offer enhanced level of contrast between different dielectrics. Due to the high cost of phase measurements, a number of alternative approaches, such as indirect holography, phase retrieval algorithms and a dual probe approach, have been developed to allow phase information to be retained in amplitude only measurements [23–25].

Indirect holographic imaging consists of two stages: the recording of a sampled holographic intensity pattern and image reconstruction.

3.1. Formation of Holographic Intensity Pattern

The off-axis hologram was first introduced by Leith and Upatnieks [26] for the recording of optical wavefronts. In the recording stage, an intensity pattern is formed from the interference pattern between the scattered wavefront and a coherent plane wave, introduced at an offset angle to the recording plane. This offset hologram was first introduced by Leith and Upatnieks [26] for the recording of optical wavefronts and is illustrated in Figure 1.

The adoption of this technique at microwave frequencies has proved difficult due to the practical problems associated with providing an offset reference wave. A technique to overcome this problem has been described [27, 28]. The basis of this technique is to replace the offset radiated reference wave by an electronically synthesized reference wave. This is derived by tapping off a fraction of the signal used to illuminate the object using a directional coupler. The phase of this signal is controlled by varying the phase shifters under computer control. To form an intensity pattern, the reference signal is combined

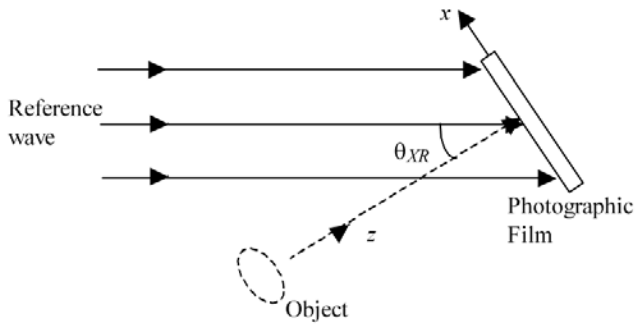

Figure 1. Off-axis hologram.

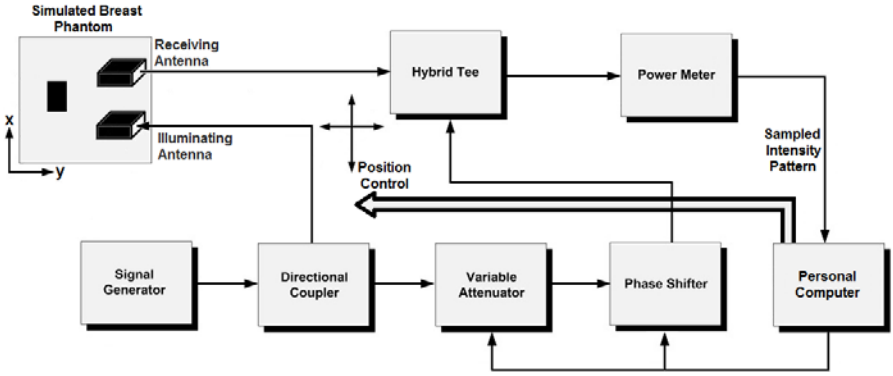

Figure 2. Experimental arrangement for intensity pattern formation.

with the scattered signal of the object. A diagrammatic representation of this arrangement is shown in Figure 2.

The form of the resultant intensity pattern, which is measured in the spatial domain as a function of measurement plane axis parameters, $I(x, y)$, is given by:

$$\begin{aligned} I(x,y) &= |E(x,y) + R(x,y)|^2 \\ &= |E(x,y)|^2 + |R(x,y)|^2 + E(x,y)R^*(x,y) + E^*(x,y)R(x,y) \end{aligned} \quad (4)$$

where $E(x, y)$ represents the complex scattered field over the x-y plane, $R(x, y)$ the complex field of the reference wave over the x-y plane, and $*$ denotes complex conjugate. If the reference wave is introduced along the x axis, it takes the form:

$$R(x,y) = E_0 e^{-jk_x x} \quad (5)$$

$$R^*(x,y) = E_0 e^{jk_x x} \quad (6)$$

3.2. Image Reconstruction

The first stage in the process to reconstruct a high quality image of the original object is to take the Fourier transform of this intensity pattern given in Equation (4) to obtain a pattern in the spatial frequency domain as given in Equation (7).

$$\begin{aligned} F\{I(x,y)\} &= F\left\{|E(x,y)|^2\right\} + F\left\{|R(x,y)|^2\right\} \\ &\quad + F\{E(x,y)\} \otimes F\{R^*(x,y)\} \\ &\quad + F\{E^*(x,y)\} \otimes F\{R(x,y)\} \end{aligned} \quad (7)$$

Provided that the spatial frequency of the scattered object is band limited and a sufficient phase shift can be applied to the reference

wave, the four components in Equation (7) can be separated into three regions. This is shown diagrammatically in Figure 3.

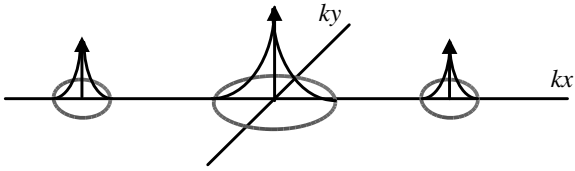

Figure 3. Spectral representation of an off-axis hologram.

The first two terms of Equation (7) correspond to the auto-correlation of the scattered object wave and the reference wave, respectively. These components appear in the centre of the spectrum as a result of their DC content. The third and fourth terms of Equation (7) relate to the convolution of the reference wave with the scattered wave and its complex conjugate. These are offset from the origin by an amount related to the angle of the reference wave and contain sufficient information to reconstruct the image. The use of a synthesised offset reference plane wave allows the third and fourth terms of Equation (7) to be separated in the spatial frequency domain. The next stage in the reconstruction process is to filter off the unwanted terms and centralise the required term to give the PWS of the original object:

$$F'\{(x,y)\} = E_0 \cdot F\{E(x,y)\} \tag{8}$$

Taking the inverse Fourier transform of Equation (8) gives the original scattered field of the object at the measurement plane, $z = 0$:

$$G\left\{F'\{I(x,y)\}\right\} = E_0 \cdot E(x,y) \tag{9}$$

A focused image of the object at different distances can be obtained by back-propagating the PWS of the object given in Equation (8) through the desired distance, $z = d$ [19]. This particular step follows the same approach to that described for direct holography in Equation (2) in Section 2.

4. APPLICATION TO BREAST CANCER DETECTION

4.1. Simulated Breast Phantom

To demonstrate the ability of this technique to produce good quality images, a simulated breast phantom, similar to that adopted by Fear et al. [7] for experiments on simulated breast tumors, has been

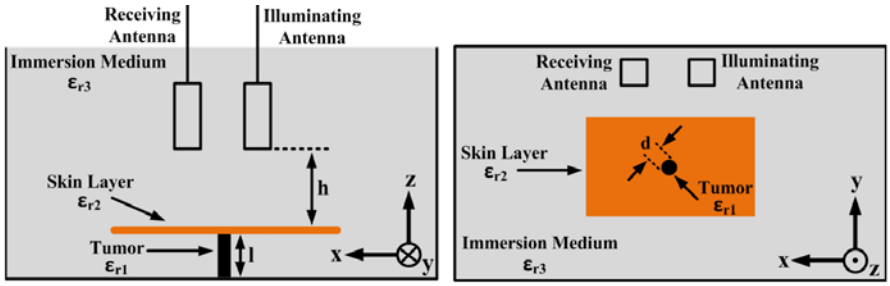

Figure 4. Simulated breast phantom, (a) front view, x-z plane, (b) top view, x-y plane ($\varepsilon_{r1} = 11.9$, $\varepsilon_{r2} = 4.5$, $\varepsilon_{r3} = 2$, $l = 6\,\text{cm}$, $d = 4\,\text{cm}$, $h = 10\,\text{cm}$).

adopted. The breast phantom, shown in Figure 4, emulates a system configuration where a patient is lying in a supine position with transmit and receive antennas placed near the surface of the naturally flattened breast. A bath of vegetable oil, with a dielectric constant ε_{r3} of 2, is used to represent both the immersion liquid and the healthy breast tissue. The use of immersion liquid significantly reduces the reflection at the air-skin interface [7]. The skin layer is constructed as a sheet of PCB FR4, with a dielectric constant ε_{r2} of 4.5 and dimensions $L = 60\,\text{cm}$, $W = 30\,\text{cm}$ and thickness of 1.57 mm. To represent the tumor, a cylindrical sheet of silicon with a dielectric constant ε_{r1} of 11.9 and dimensions $l = 6\,\text{cm} \times r = 2\,\text{cm}$ is placed on the underside of the PCB sheet. It should be noted here that the length of the tumor, which is in the z-axis in Figure 4(a), was chosen as 6 cm to make it easier to mount the tumor within the breast phantom and this selection is not a crucial parameter for the success of the imaging method due to the 2D scan over the x-y plane as illustrated in Figure 4(b). In the classification of the tumor size, which is 4 cm in diameter in the x-y plane in Figure 4(b), the Tumor size-Node-Metastasis (TNM) classification method was used [29]. In this classification method, a tumor which has not spread to the lymph nodes within the breast and has a size of larger than 2 cm but smaller than 5 cm corresponds to Stage 2A breast cancer, which is accepted as the last phase of the early stage. The dielectric properties of the breast phantom used in this work, which were obtained from [7], are in agreement with the recently published work on breast cancer research [11, 30, 31].

4.2. Experimental Arrangement

The system illustrated in Figure 2 and Figure 5 was used to generate an image of the breast phantom. Two open-ended WR-90 probes were used to illuminate and receive the scattered signal from the breast phantom. Experimental results have shown mutual coupling between both probes can be minimized by having a separation between the probes of 6 cm. In order to improve the impedance matching between the probes and the immersion liquid, both probes were also fully immersed in liquid. A coherent reference wave is derived by tapping off a fraction of the signal used to illuminate the object using a directional coupler. The phase of this signal is controlled by varying the phase shifters under computer control. This signal is combined with the signal scattered from the object. The intensity of the combined signal is recorded using a microwave power meter.

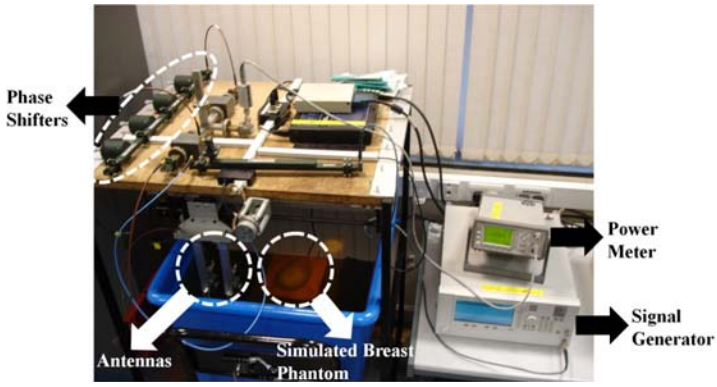

Figure 5. Photograph of experimental system.

4.3. Experimental Results

Results were taken over a scanning aperture of 40 cm × 40 cm, at a distance h of 10 cm from the object. An operating frequency of 9.4 GHz and a sample spacing, $dx = dy = 1$ cm were used. At 9.4 GHz, the electrical length of the sample spacing is less than a half-wavelength in the vegetable oil immersion medium, 1.13 cm, providing good resolution reconstruction of amplitude and phase images. Another factor to be considered is the coupling of the microwave power into the breast tissue, which presents a significant challenge at microwave frequencies due to the electrical properties of living tissues in human body. This can be overcome by using a coupling medium in which both

the antennas and the imaged tissue are immersed [10]. A solution to this challenge was adopted in [3, 13] where corn syrup was selected as the coupling medium providing very similar dielectric constants to the breast tissues examined in [7]. It was demonstrated in [3, 13] that this selection significantly reduces the total propagation loss, which consists of dissipation loss and diffusion loss. In this work, vegetable oil was selected as the coupling medium providing similar dielectric constant to the breast tissues examined in [7, 30]. This selection decreases the propagation loss in the immersion medium and the breast tissue and reduces the reflection at the air-skin interface [7]. The resultant measured holographic intensity pattern is shown in Figure 6.

To reconstruct an image of the tumor, the intensity pattern is processed using the theory described in Section 3.2. The intensity pattern first has its DC component removed and then is zero buffered to four times its original length before being Fourier transformed in order to improve smoothing. In reconstructing the original object, the vegetable oil medium has been assumed to be lossless. The resultant plane wave spectrum of the intensity pattern is shown in Figure 7, with the required spectrally filtered data highlighted.

From this data, magnitude and phase plots of the tumor have been reconstructed and are shown in Figure 8(a) and Figure 8(b), respectively. Examining both plots illustrated in Figure 8, the three regions of oil, PCB and silicon (fat, skin and tumor) can clearly be seen with the tumor highlighted. Whilst it may be difficult to discern the tumor from the amplitude image in Figure 8(a) due to poor scattering response of dielectric silicon, a clear outline of the tumor can be

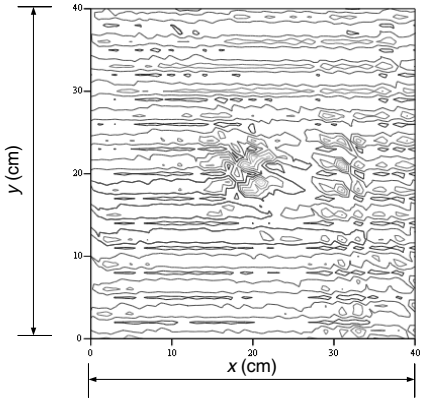

Figure 6. Recorded holographic intensity pattern.

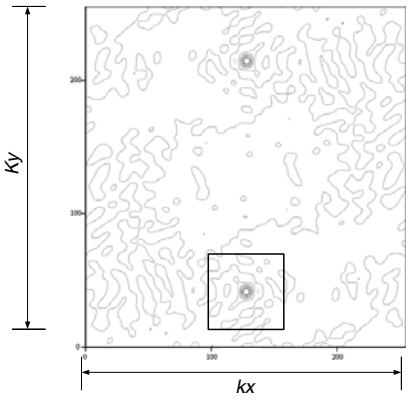

Figure 7. Spectral distribution.

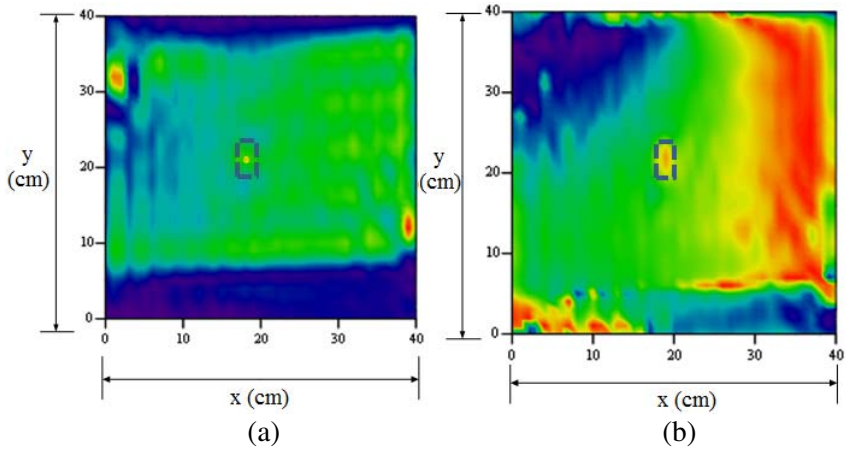

Figure 8. Reconstructed images of the breast phantom with the tumor highlighted, (a) magnitude image, (b) phase image.

discerned from the reconstructed phase image in Figure 8(b). Please note, the two red segments shown in opposite corners of the magnitude are a result of the supporting structure used to secure the PCB in the immersion medium.

In order to demonstrate the resolution limits of the imaging method, the indirect holographic scanning of two 5p British coins with a diameter of 1.6 cm, which equates to a half-wavelength in free space at 9.4 GHz, was performed over a scanning aperture of 21 cm × 21 cm. The coins were placed upon an RF absorber and separated by a distance of 6 cm from each other. The reconstructed amplitude and phase images of the coins are illustrated in Figure 9.

As illustrated in Figure 9, the reconstructed amplitude and phase images of the coins demonstrate good resolution. A clear contrast can be seen between the scanning aperture background and the coins in the reconstructed amplitude image in Figure 9(a) and the outlines of the coins are evident in the reconstructed phase image in Figure 9(b). This demonstrates the ability of this imaging method to reconstruct the images of a scanned object with a resolution of a half-wavelength.

5. INDIRECT HOLOGRAPHIC STEREOSCOPIC IMAGING

The technique described so far in this paper involves the use of a single frequency CW signal. Whilst this approach can provide good

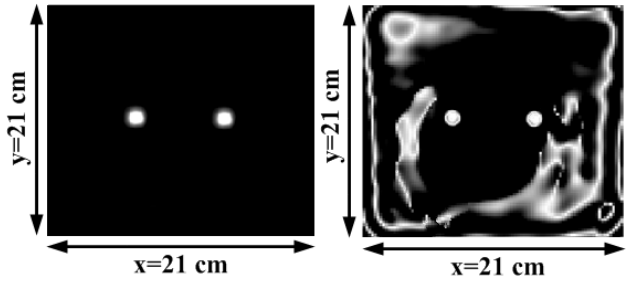

Figure 9. Reconstructed images of two 5p British coins with a diameter of 1.6 cm, (a) magnitude image, (b) phase image.

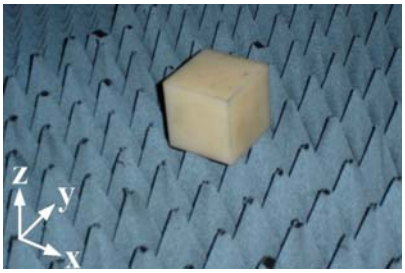

Figure 10. Test object (dielectric cube) for stereoscopic imaging.

resolution in two dimensions, a limitation of this approach is its ability to provide good resolution in the third dimension. In this section, a method of improving the depth resolution is proposed, central to which is the use of stereoscopic holographic imaging. To illustrate the reconstruction procedure, a 5 cm dielectric cube in free space, shown in Figure 10, is used as a test object.

The first stage involves taking a holographic interference pattern along the x-y plane. The procedure outlined in Section 3 is then used to reconstruct multiple 2D slices at different depths in the z-direction. These are illustrated in Figure 11(a). An orthogonal holographic interference pattern, along the x-z plane, was also measured. The same reconstruction process was used to produce multiple 2D slices, at different depths along the y-direction. These are shown in Figure 11(b).

The two cubes of data are then combined to produce a 3D image, as shown in Figure 12.

As can be seen in Figure 12, the Indirect Stereoscopic Holographic Imaging technique provides good depth resolution in addition to 2D

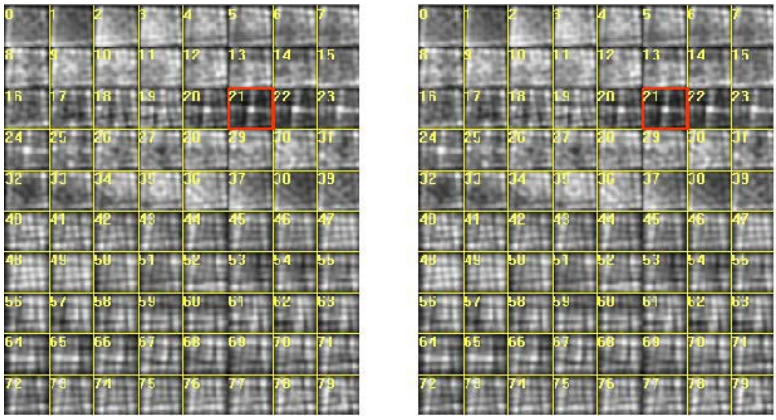

(a) (b)

Figure 11. Reconstructed slices, (a) along z-axis, reconstructed from intensity measurements taken along the x-y plane, (b) along y-axis, reconstructed from intensity measurements taken along the x-z plane.

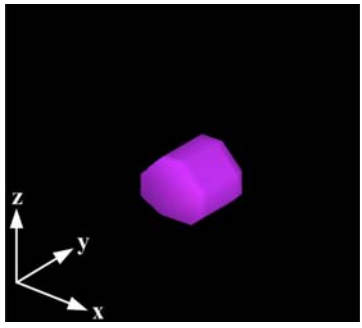

Figure 12. Reconstructed 3D image of cube.

plane resolution enabling the proposed technique to be employed in medical imaging applications where resolution in all three dimensions (x, y, and z) is of interest. It should be noted here that the 3D shape approximation performance of the technique can easily be improved by increasing the number of 2D slices.

6. CONCLUSION

A new technique for the detection of breast cancer based on a novel indirect holographic technique has been demonstrated. Practical results have shown that this technique is successful for determining both the location and shape of the simulated tumor. The use of

this approach offers considerable benefits in terms of simplicity and expense when compared with other microwave imaging techniques. Recent experimental results have also demonstrated that limited depth resolution, which is a recognized consequence of single frequency CW imaging, can be overcome through the use of stereoscopic holographic imaging.

REFERENCES

1. Pisano, E. D., C. Gatsonis, E. Hendrick, M. Yaffe, J. K. Baum, S. Acharyya, E. F. Conant, L. L. Fajardo, L. Bassett, C. D'Orsi, R. Jong, and M. Rebner, "Diagnostic performance of digital versus film mammography for breast-cancer screening," *The New England Journal of Medicine*, Vol. 353, No. 17, 1773–1783, 2005.
2. Artmann, A., K. Hellerhoff, and S. H. Heywang-Kobrunner, "Screening in women with increased breast cancer risk," *Breast Care*, Vol. 1, No. 1, 22–25, 2006.
3. Bindu, G. N., S. J. Abraham, A. Lonappan, V. Thomas, C. K. Aanandan, and K. T. Mathew, "Active microwave imaging for breast cancer detection," *Progress In Electromagnetics Research*, Vol. 58, 149–169, 2006.
4. O'Halloran, M., M. Glavin, and E. Jones, "Rotating antenna microwave imaging system for breast cancer detection," *Progress In Electromagnetics Research*, Vol. 107, 203–217, 2010.
5. Zhou, H., T. Takenaka, J. E. Johnson, and T. Tanaka, "A breast imaging model using microwaves and a time domain three dimensional reconstruction method," *Progress In Electromagnetics Research*, Vol. 93, 57–70, 2009.
6. Zhang, H., S. Y. Tan, and H. S. Tan, "A novel method for microwave breast cancer detection," *Progress In Electromagnetics Research*, Vol. 83, 413–434, 2008.
7. Fear, E. C., X. Li, S. C. Hagness, and M. A. Stuchly, "Confocal microwave imaging for breast cancer detection: Localization of tumors in three dimensions," *IEEE Transactions on Biomedical Engineering*, Vol. 49, No. 8, 812–822, Aug. 2002.
8. Fear, E. C., S. C. Hagness, P. M. Meaney, M. Okoniewski, and M. A. Stuchly, "Enhancing breast tumour detection with near-field imaging," *IEEE Microwave Magazine*, Vol. 3, No. 1, 48–56, Mar. 2002.
9. Hagness, S. C., A. Taflove, and J. E. Bridges, "Two dimensional FDTD analysis of a pulsed microwave confocal system for breast cancer detection: Fixed focus and antenna array sensors," *IEEE*

Transactions on Biomedical Engineering, Vol. 45, No. 12, 1470–1479, Dec. 1998.

10. Nikolova, N. K., "Microwave imaging for breast cancer," *IEEE Microwave Magazine*, Vol. 12, No. 7, 78–94, Dec. 2011.
11. Conceicao, R. C., M. O'Halloran, M. Glavin, and E. Jones, "Comparison of planar and circular antenna configurations for breast cancer detection using microwave imaging," *Progress In Electromagnetics Research*, Vol. 99, 1–20, 2009.
12. Maskooki, A., E. Gunawan, C. B. Soh, and K. S. Low, "Frequency domain skin artifact removal method for ultra-wideband breast cancer detection," *Progress In Electromagnetics Research*, Vol. 98, 299–314, 2009.
13. Bindu, G. N., A. Lonappan, V. Thomas, C. K. Aanandan, and K. T. Mathew, "Dielectric studies of corn syrup for applications in microwave breast imaging," *Progress In Electromagnetics Research*, Vol. 59, 175–186, 2006.
14. Rosen, A., M. A. Stuchly, and A. V. Vorst, "Applications of RF/microwaves in medicine," *IEEE Transactions on Microwave Theory and Techniques*, Vol. 50, No. 3, 963–974, Mar. 2002.
15. Karpowicz, N., H. Zhong, J. Xu, K. Lin, J. S. Hwang, and X. C. Zhang, "Comparison between pulsed terahertz imaging time-domain imaging and continuous wave terahertz imaging," *Semiconductor Science and Technology*, Vol. 20, No. 7, 293–299, Jul. 2005.
16. Smith, D., "Microwave holographic measuring method and apparatus," Patent Application, No. 0022503.7, UK, Sep. 2000.
17. Elsdon, M., D. Smith, M. Leach, and S. J. Foti, "Experimental investigation of breast tumor imaging using indirect microwave holography," *Microwave and Optical Technology Letters*, Vol. 48, No. 3, 480–482, Mar. 2006.
18. Rahmat-Samii, Y., L. I. Williams, and R. G. Yaccarino, "The UCLA bi-polar planar near-field antenna measurement and diagnostic range," *IEEE Antennas and Propagation Magazine*, Vol. 37, No. 6, 16–35, Dec. 1995.
19. Yaghjian, A. D., "An overview of near-field antenna measurements," *IEEE Transactions on Antennas Propagation*, Vol. 34, No. 1, 30–45, Jan. 1986.
20. Smith, D., M. Leach, M. Elsdon, and S. J. Foti, "Indirect holographic techniques for determining antenna radiation characteristics and imaging aperture fields," *IEEE Antennas and Propagation Magazine*, Vol. 49, No. 1, 54–67, Feb. 2007.

21. Yurduseven, O., D. Smith, B. Livingstone, V. Schejbal, and Z. You, "Investigations of resolution limits for indirect microwave holographic imaging," *International Journal of RF and Microwave Computer-Aided Engineering*, Vol. 23, No. 4, 410–416, Jul. 2013.
22. Leach, M., M. Elsdon, S. J. Foti, and D. Smith, "Imaging dielectric objects using a novel off-axis holographic technique," *Microwave and Optical Technology Letters*, Vol. 48, No. 1, 1957–1959, Oct. 2006.
23. Gabor, D., "Microscopy by reconstructed wavefronts," *Proceedings of the Royal Society of London (Series A)*, Vol. 197, No. 1051, 454–487, Jul. 1949.
24. Tenant, A., G. Junkin, and A. P. Anderson, "Advances in phase retrieval metrology," *8th International Conference on Antennas and Propagation*, Vol. 1, 323–326, 1993.
25. Gostanzo, S., G. D. Massa, and M. D. Migliore, "A novel hybrid approach for far-field characterization from near-field amplitude-only measurements on arbitrary scanning surfaces," *IEEE Transactions on Antennas and Propagation*, Vol. 53, No. 6, 1866–1874, Jun. 2005.
26. Leith, E. N. and J. Upatnieks, "Reconstructed wavefronts and communication theory," *Journal of the Optical Society of America*, Vol. 52, No. 10, 1123–1128, Oct. 1962.
27. Brown, J. and E. V. Jull, "The prediction of aerial radiation patterns from near field measurements," *Proceedings of the IEE — Part B: Electronic and Communication Engineering*, Vol. 108, No. 42, 635–644, Nov. 1961.
28. Paris, D. T., W. M. Leach, and E. B. Joy, "Basic theory of probe-compensated near-field measurements," *IEEE Transactions on Antennas and Propagation*, Vol. 26, No. 3, 373–379, May 1978.
29. Dixon, M. and R. Sainsbury, *Handbook of Diseases of the Breast*, 2nd Edition, Churchill Livingstone, 1998.
30. Lazebnik, M., D. Popovic, L. McCartney, C. B. Watkins, M. J. Lindstrom, J. Harter, S. Sewall, T. Ogilvie, A. Magliocco, T. M. Breslin, W. Temple, D. Mew, J. H. Booske, M. Okoniewski, and S. C. Hagness, "A large-scale study of the ultrawideband microwave dielectric properties of normal, benign and malignant breast tissues obtained from cancer surgeries," *Physics in Medicine and Biology*, Vol. 52, No. 20, 6093–6115, 2007.
31. Kim, T.-H. and J.-K. Pack, "Measurement of electrical characteristics of female breast tissues for the development of the breast cancer detector," *Progress In Electromagnetics Research C*, Vol. 30, 189–199, 2012.